Volume 1 | Number 1 | Jan 2013 | Pages 1–100

Nanoscale

www.rsc.org/nanoscale

ROYAL SOCIETY OF CHEMISTRY

www.rsc.org/nanoscale

Journal Name

COMMUNICATION

Iron oxide nanoparticles protected by NIR-active multidentate-polymer as multifunctional nanoprobes for NIRF/PA/MR trimodal imaging

Yayun Wu,[†a] Duyang Gao,[†a, c] Pengfei Zhang,*[a, d] Chuansheng Li,[a] Qian Wan,[b] Chi Chen,[a] Ping Gong,[a] Guanhui Gao,[a] Zonghai Sheng[a] and Lintao Cai*[a]

We designed and synthesized a new kind of near-infrared catechol-based multidentate polymers which were intended to yield compact NIR-active iron oxide nanoparticles with excellent stability and biocompatibility. The resulted multifunctional nanoprobes showed great potential as multimodal contrast agents for NIRF/PA/MR trimodal imaging in vivo.

Molecular imaging technologies, including magnetic resonance imaging (MRI), near-infrared fluorescent imaging (NIRF), and photo-acoustic tomography (PAT), etc, have been developed to image the structure and function of biological systems for potential clinical applications and provided critical information to visualize the abnormal state of the body and monitor biological situations at the target site.[1] However, each imaging modality has its own unique advantages along with intrinsic limitations which make it difficult to obtain accurate and reliable information at the disease site. MRI is the most widely used imaging technique for human medicine, but it suffers from low spatial resolution. In contrast, NIRF imaging has high resolution and allows spatial visualization, but its application is limited by poor tissue penetration. Photoacoustic (PA) imaging as a synergistic combination of optical and ultrasound imaging technologies, provides unprecedented advantages of the high contrast of optical imaging as well as the high resolution of acoustic imaging at centimetre penetration depth, and photoacoustic-based probes is still needed to be developed. Multimodal imaging, a technique where two or more imaging modalities are combined to obtain specific advantages of various methods simultaneously, is desirable to allow precise and fast diagnosis of disease.[2] The design of multifunctional probes for multimodal imaging and integrated with chemotherapy drugs or target molecules have attracted a lot interests, as it is possible to obtain multiple imaging data using the advantages of each modality, simultaneous diagnosis and therapy.[3]

Recent advances in nanobiotechnology have contributed to the development of nano-sized multimodal contrast agent through combining multiple discrete components into a single multifunctional nanoparticle.[4] As one of the FDA-Approved nanoparticles, superparamagnetic iron oxide (SPIO) nanoparticles have shown great potentials for various biomedical and clinical applications, including biosensing, medical imaging, and drug delivery, because of their unique magnetic property, chemical stability and biocompability.[5] Most effective synthetic strategies that provide high-quality magnetic nanocrystals are based on high temperature reaction of organometallic precursors, which resulted as-prepared nanoparticls capped with long chain hydrophobic ligands (such as oleylamine, oleic acid) and dispersible in organic solvent.[6] Therefore, the surface engineering of iron oxide nanoparticles played an essential role in not only improving their hydrophilicity and stability, but also introducing various specific active motifs to produce functionalized contrast agents for biomedical imaging.[7]

During the past few years, various strategies have been developed for surface modification of hydrophobic nanoparticles, which could be traditionally classified into two categories: surface coating and ligand exchange.[8] However, each has its own merits. Instead, multidentate polymer ligands exhibited stronger anchoring properties and provided an alternative route to produce compact hydrophilic nanoparicles with highly stability.[9] Especially, catechol-derived dopamine-based polymeric ligands have successfully been developed as high-affinity anchors for nanoparticle surface engineering.[10] Herein, we designed and synthesized a new set of near-infrared multidentate polymers that which were intended to yield compact NIR-active iron oxide nanoparticles with excellent stability. We further combined the multifunctional nanoprobes with near-infrared fluorescence (NIRF), photo-acoustic (PA), magnetic resonance (MR) multimodal imaging techniques for in vivo sentinel lymph node imaging.

[a.] *Guangdong Key Laboratory of Nanomedicine, CAS Key Laboratory of Health Informatics, Shenzhen Bioactive Materials Engineering Lab for Medicine, Institute of Biomedicine and Biotechnology, Shenzhen Institutes of Advanced Technology, Chinese Academy of Sciences. Shenzhen, 518055, P. R. China. E-mail: lt.cai@siat.ac.cn.*
[b.] *Paul C. Lauterbur Research Center for Biomedical Imaging, Institute of Biomedical and Health Engineering, Shenzhen Institutes of Advanced Technology, Chinese Academy of Sciences, Shenzhen 518055, P.R. China.*
[c.] *Bioimaging Core, Faculty of Health Sciences, University of Macau, Macao, China*
[d.] *Division of Biomedical Engineering, The Hong Kong University of Science and Technology, Clear Water Bay, Kowloon, China. E-mail: pzhangad@connect.ust.hk.*
† These authors contributed equally.
Electronic Supplementary Information (ESI) available: [details of experiment and Figure S1-S6]. See DOI: 10.1039/x0xx00000x

As depicted in Scheme 1 and Figure S1, the NIR-emitting multidentate polymers (820-PIMA-Dopa) were produced using poly (isobutylene-alt-maleic anhydride)(PIMA) as backbone, dopamine as coordinating moieties, and Indocyanine Green analogues (IR-820) were linked through cysteamine as NIR optical-active moieties. Water-soluble IONPs capped with 820-PIMA-Dopa (noted as IONPs@820-PIMA-Dopa, here after) were prepared by displacing the native ligands on the initial hydrophobic iron oxide NPs with the dopamine groups along the polymer backbone, which produced a dramatic enhancement in the ligand affinity to nanoparticles. This ligand design was built on the high reactive efficiency of the addition reaction between anhydride rings and amine groups, which facilitated the quantitatively controlled one-step reaction and incorporation of specific active groups.[11] IR-820 cyanine dye was chosen due to its unique absorption bands and photoluminescence in the near-infrared wavelength range and related lower toxicity.[12] Due to the fragile structure of NIR dyes, the chemical modification was not straightforward. In an effort to develop a convenient method to introduce IR-820 into the polymeric anhydride, replacing the meso-halogen in the dye structure was substituted by cysteamine in one pot, which provided the further conjugation between the dye and the polymer backbone.[13] The average number of monomers per PIMA chain (or index of polymerization) is equal to ~40. Typically, 50% of the maleic anhydride rings (~ 20 units) in the polymer chain were used for reaction with dopamine, leaving the other 50% for reaction with cysteamine. The thiol group of cysteamine was used to conjugate IR 820 via replacing chlorine in the cyclohexenyl ring. This was expected to introduce a total of ~40 dopamines and cyestamine moieties (which ensured that there were enough anchoring groups for effective coordination onto the NP surface and thiol groups for IR 820 conjugation), while freeing ~40 carboxyl groups along the polymer chain (which provided additional hydrophilic and potential reactive groups in the final compound). After simply mixing PIMA, dopamine and cysteamine with triethylamine as activating reagents in DMSO solvent and heated to 80°C overnight. And then, IR-820 was added to react for further 12 hours. It should be pointed out that all the reactions were completed in one pot in high yields. The final product could be easily acquired by dialyzing and freeze-drying to obtain blue powder without further purification, which were characterized using ^{1}H NMR spectroscopy (Figure S2). The ^{1}H NMR

spectra (in DMSO-d_6) showed a multiplet peak at 6.4-6.7 ppm (attributed to the aromatic protons from catechol) and a broad peak around 1.1 ppm ascribed to protons of methyl groups in the polymer. The weak mulitplet peak at 7.3-8.2 ppm was attributed to the aromatic protons from IR 820. The stoichiometry of the ligand for each component was estimated from the corresponding ^{1}H NMR spectrum. The CH_3 terminal signals of polymer at 1.1 ppm were used as a backbone reference; the three aromatic protons per catechol at 6.4-6.7 ppm were used to calculate the number of dopamine and the CH_3 signal from the heterocyclic dye at 1.6-1.9 ppm range was used to calculate the number of IR-820. From the intergration, we measured ~19 dopamines (59.70 H, ~100%) per polymer chain (234 H) for PIMA-Dopa polymer and ~20 dopamines(61.15 H, ~100%),~ 6 IR 820 (74.91 H, ~75%). Overall, the above analysis indicated that the coupling efficiency between maleic anhydride and dopamine was essentially 100% complete, and IR 820 was successfully linked to the polymer very efficiently (~75%).

Organic-soluble iron oxide NPs capped with oleyamine (IONPs@OA) were synthesized and transferred into water using the 820-PIMA-Dopa polymers following the previously established protocols.[14,11] The as-prepared 820-PIMA-Dopa capped IONPs showed excellent magnetic and NIR optical properties (Figure 1a, 1b). To directly demonstrate magnetic and optical properties of as-prepared 820-PIMA-Dopa capped nanoparticles, IONPs@OA and IONPs@820-PIMA-Dopa were placed in a water/chloroform biphasic system in glass vials with a magnet aside. An obviously liquid surface deformation of IONPs@OA in chloroform and IONPs@820-PIMA-Dopa in water were displayed. In addition, the high fluorescence of IONPs@820-PIMA-Dopa in water phase also demonstrated the excellent NIR-active property. FT-IR spectrum of the original IONPs@OA and the as-received water-soluble IONPs@820-PIMA-Dopa (Figure 1c) clearly showed displacement of oleylamine shell by the 820-PIMA-Dopa after phase transfer. Magnetic measurements indicated superparamagnetic behaviour at room temperature for as-prepared hydrophilic nanoparticles, which were similar to the original hydrophobic nanoparticles (Figure 1d and Figure S3). As shown in Figure 1e, the absorption and photoluminescence spectrum of IONPs@820-PIMA-Dopa displayed the absorbance at ~680 nm and major emission peak at ~762 nm, which was blue-shift from the original emission of 812 nm of IR-820 dye. Such phenomenon could be attributed to the electronic state alteration in the dye molecules.[13] As shown in Table S1, The quantum yield of as-prepared IONPs@820-PIMA-Dopa was measured to be 1.196% (ICG dye with quantum yield of 13% was used as the standard), which was 1.5 times compared to the IR-820 in water (with the quantum yield of 0.783%). The enhancement of photoluminescence of IR-820 may be attributed to the polymer protected the dye molecules from aqueous solution. The TEM images (Figure S4) indicated that these nanoparticles with radius ~7 nm were spherical with uniform cores and narrow size distribution. Through the dynamic light scattering (DLS) data, IONPs@820-PIMA-Dopa also showed narrow size distribution and compact hydrodynamic size (~20 nm) (Figure 1.f), which were larger compared to their overall dimensions from TEM measurements because of a dense polymeric coating. Nearly every individual nanocrystal was found to be coated with a uniform shell with an
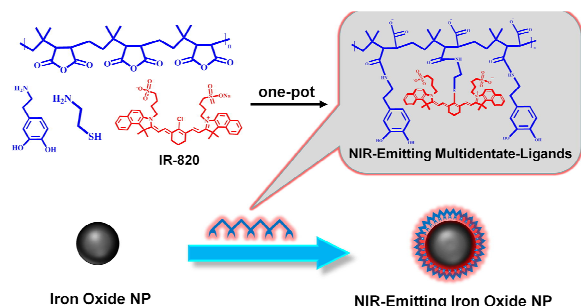
Scheme 1. Schematic illustration of the synthesis of the near-infrared catechol-based multidentate polymers 820-PIMA-Dopa and the procedure to prepare 820-PIMA-Dopa coated IONPs.
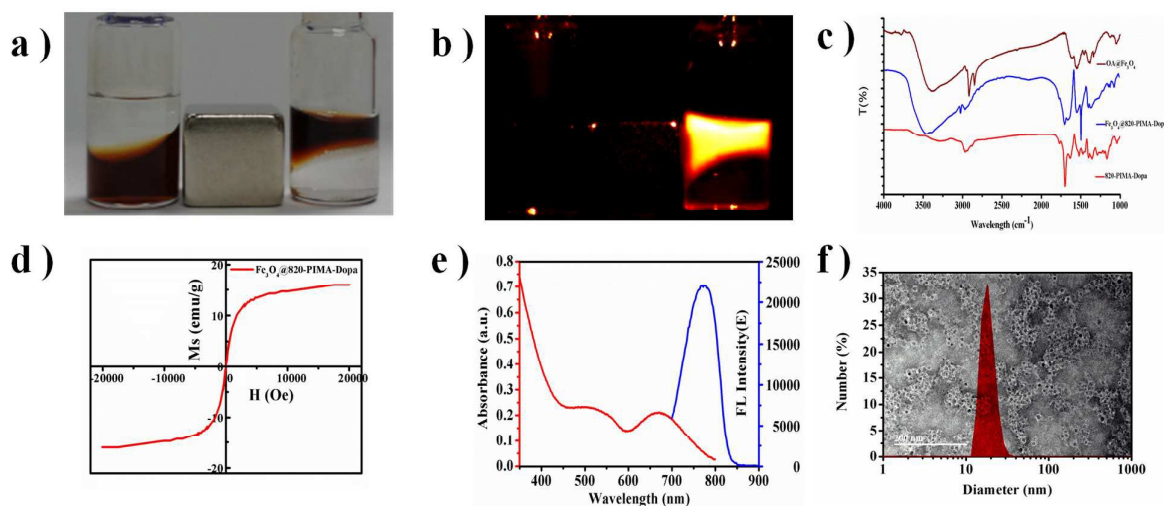
Figure 1. a) Photos of IONPs before (left) and after (right) coating with 820-PIMA-Dopa near a magnet. b) NIR Fluorescence photos of the IONPs before (left) and after (right) coating with 820-PIMA-Dopa under xenon lamp equipped with filter to provide NIR excitation. Upper layer is H_2O and lower layer is $CHCl_3$. c) FTIR spectra of IONPs before (left) and after (right) coating with 820-PIMA-Dopa. d) Magnetic hysteresis loop of IONPs@820-PIMA-Dopa at 300 K. e) UV/Vis absorption spectra and photo-luminescence spectra of IONPs@820-PIMA-Dopa. f) TEM image and DLS size distribution of IONPs@820-PIMA-Dopa.

average thickness of ~7 nm. TGA has been performed to confirm the coating formation and estimate the binding efficiency on the surface of NPs(Figure S5). A slight weight loss was observed up to 200 °C in IONPs@820-PIMA-Dopa curve, probably duo to absorbed water, while a significant weight loss took place between 200 and 450 °C. The weight loss for IONPs@OA, attributed to decomposition of oleyamine, was about 16.2%, corresponding to a monolayer of oleyamine on the surface. The weight loss for IONPs@820-PIMA-Dopa was increased to 57.7%, mainly due to the decomposition of 820-PIMA-Dopa polymer.

We next evaluated the colloidal stability and photostability stability of as-prepared nanoparticles using dynamic light scattering and fluorescent spectrometer, respectively. The results showed these NIR-emitting nanoparticles stayed stable in buffers over a broad range of pH (pH 6-11) and in the presence of added excess electrolytes (up to 2 M NaCl) (Figure 2a-2d). Interestingly, free IR-820 dyes were precipitate in buffer with pH ranging from 4 to 10 or in NaCl solution and displayed very low fluorescent intensity (Figure S6). However, our strategy of linking IR-820 to polymer backbone significantly enhanced the stability of organic dye. Further photostability experiment and storage stability assay also confirmed our statements(Figure S7). To evaluate the cytotoxicity of IONPs@820-PIMA-Dopa, CCK-8 assay was carried out on MCF-7 cells in presence of NPs with different concentrations (Figure 2f). There was no significant change in cell proliferation for IONPs@820-PIMA-Dopa (200 μg/mL nanoparticles highest concentration tested). 820-PIMA-Dopa polymer-coated IONPs in glass vials were also left at room temperature under various conditions to monitor the shelf life in a normal working environment. All the samples showed good colloidal stability for long time periods(Figure S8).

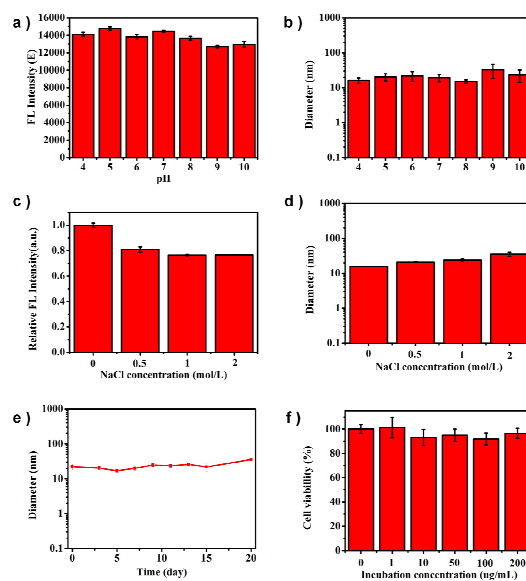Overall, the above data confirmed that as-prepared nanoparticles hold great

Figure 2. The stability and biocompatibility results of IONPs@820-PIMA-Dopa. a) Fluorescence and b) colloidal stability tests of IONPs@820-PIMA-Dopa in various pH buffers. c) Fluorescence and d) colloidal stability tests of IONPs@820-PIMA-Dopa under various concentrations of NaCl solutions. e) the storage stability experiment of IONPs@820-PIMA-Dopa. f) Cytotoxicity experiments of IONPs@ 820-PIMA-Dopa. MCF-7 cells were incubated with nanoparticles at

different concentrations ranging from 0 to 200 µg/ml for 24 hours. Error bars represent standard deviations from multiple trials.

stability and biocompatibility, which were very promising for further biological applications.

We further examined whether IONPs@820-PIMA-Dopa could be applied as multimodal contrast agents. The NIRF imaging demonstrated that the fluorescent IONPs showed emission peaks at 780 nm and could be easily separated from autofluorescence (Figure 3a). From the in vitro MRI measurements we observed reduced signals in T_2-weighted MR images with increased metal concentrations of IONPs@820-PIMA-Dopa nanoparticles, the T_2 relaxation rate ($1/T_2$) was linearly fitted as a function of Fe concentration, and the r_2 relaxivity of IONPs@820-PIMA-Dopa was estimated to be 135.03 mM^{-1} s^{-1}, which confirmed as-prepared nanoparticles as an effective MRI contrast agent. The photoacoustic imaging capability of as-prepared NIR-active IONPs was also studied using a tissue-mimicking phantom. Figure 3c showed the corresponding photoacoustic image of a phantom loaded with nanoparticles (left) and blank control (PBS alone, right). An tunable ns-pulsed OPO laser operating at

808 nm was used as the PA excitation source considering the negligible tissue scattering and maximal penetration depth for deep tissue imaging in this region. While water produced non-detectable and relatively weak PA signals, High signal intensity from nanoparticles was observed, which indicated efficient photoacousic signal generation capability of as-prepared IONPs@820-PIMA-Dopa nanoparticles. To demonstrate that IONPs@820-PIMA-Dopa could be used for in vivo multimodal imaging, the hydrophilic NPs was injected subcutaneously into the distal part of the right anterior paw of healthy mice for regional lymph node mapping. As the IONPs@820-PIMA-Dopa travelled through the lymphatic and accumulated to the lymph
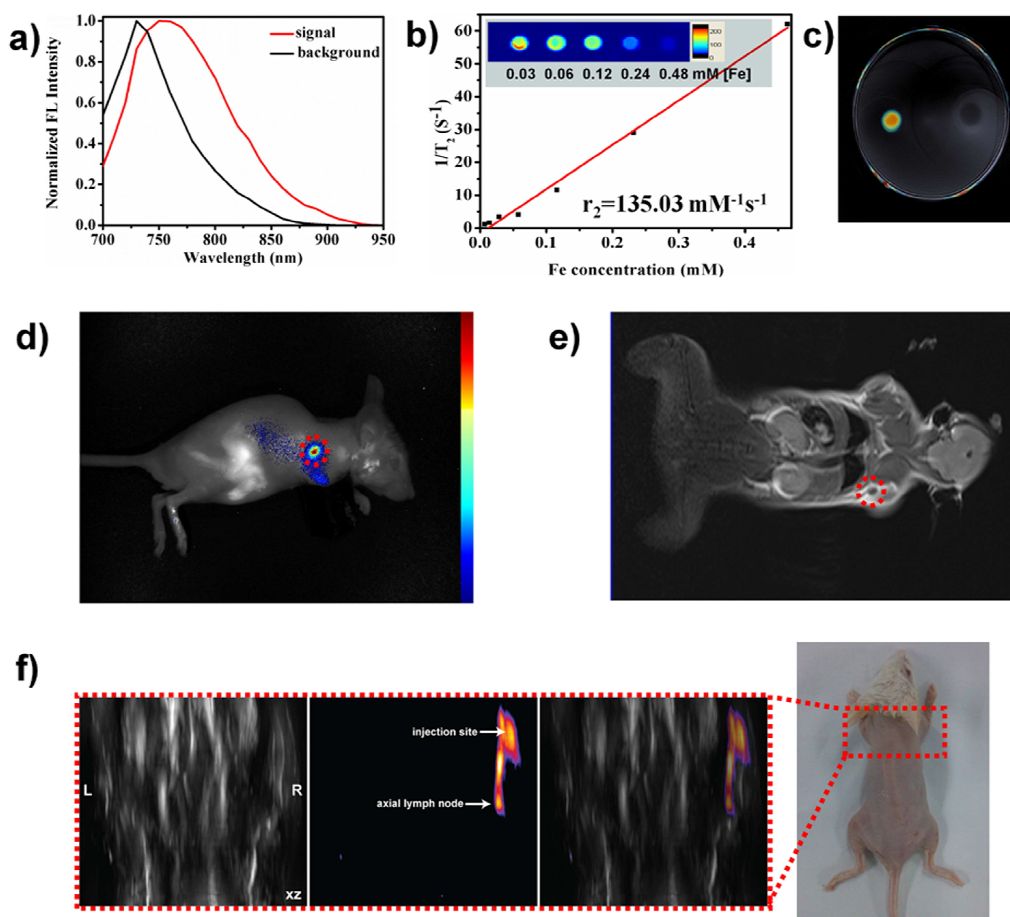

Figure 3. The NIRF/MR/PA triple-modal imaging experiments. a) NIRF spectra of IONPs@820-PIMA-Dopa (red) and autofluorescence from the mice (black) acquired with in vivo fluorescent imaging system. b) Plot of $1/T_2$ (s^{-1}) as a function of Fe concentration for IONPs@820-PIMA-Dopa. The slope indicated the specific T_2 relaxivity (135.03 mM^{-1} s^{-1}). c) In vitro evaluation of IONPs@820-PIMA-Dopa as a photoacoustic contrast agent. IONPs@820-PIMA-Dopa (left) was placed in a polyurethane phantom along with saline solution (right) as a blank. d) in vivo NIRF imaging of mouse injected with IONPs@820-PIMA-Dopa nanoparticles. e) T_2 weighted MRI of the mouse. Red circle indicate the lymph node. f) In vivo PA imaging of the mouse after injection of the IONPs@820-PIMA-Dopa in the front paw the signal can be observed in the injection site, lymph vessels and axial lymph node.

Nanoscale Accepted Manuscript

node, robust signals with different multimodality were captured after 30 minutes post-injection , which indicated the position of lymph node with NIRF/MR/PA imaging at same time.

In conclusion, we synthesized a new set of multifunctional polymer ligands that combine multiple metal-coordinating groups and NIR-active moieties in the same structure. The as-prepared multidentate polymers were intended to yield compact NIR-active iron oxide nanoparticles with excellent stability and biocompatibility, which could be potentially applied as NIRF/PA/MR multimodal contrast agents for in vivo imaging. In addition, these multidentate polymers could be extended by replace catechol groups with the other groups (mercaptan groups, imidazole groups, etc.) to modify other type of nanoparticles (such as MnO, Au, Ag, CdSe/ZnS nanostructures).

Notes and references

1   R. Weissleder, *Science*, 2006, **312**, 1168.
2   (a) J. V. Jokerst and S. S. Gambhir, *Acc. Chem. Res.*, 2011, **44**, 1050; (b) W. Cai and X. Chen, *J. Nucl. Med.*, 2008, **49**, 113S
3   (a) G. Seeta Rama Raju, L. Benton, E. Pavitra and J. S. Yu, *Chem. Commun.*, 2015,**51**,13248; (b) T.-H. Shin, Y. Choi, S. Kim and J. Cheon, *Chem. Soc. Rev.*, 2015, **44**, 4501;
4   (a) E. Huynh and G. Zheng, *Wiley. Interdiscip. Rev. Nanomed. Nanobiotechnol.*, 2013, **5**, 250; (b) S. Liu, B. Jia, R. Qiao, Z. Yang, Z. Yu, Z. Liu, K. Liu, J. Shi, H. Ouyang, F. Wang and M. Gao, *Mol. Pharmaceutics*, 2009, **6**, 1074; (c) T. Liu, S. Shi, C. Liang, S. Shen, L. Cheng, C. Wang, X. Song, S. Goel, T. E. Barnhart, W. Cai and Z. Liu, *ACS Nano*, 2015, **9**, 950; (d) Y. Ma, S. Tong, G. Bao, C. Gao and Z. Dai, *Biomaterials*, 2013, **34**, 7706; (e) D.-H. Hu, Z.-H. Sheng, P.-F. Zhang, D.-Z. Yang, S.-H. Liu, P. Gong, D.-Y. Gao, S.-T. Fang, Y.-F. Ma and L.-T. Cai, *Nanoscale*, 2013, **5**, 1624; (f) D. Gao, P. Zhang, Z. Sheng, D. Hu, P. Gong, C. Chen, Q. Wan, G. Gao and L. Cai, *Adv. Funct. Mater*., 2014, **24**, 3897.
5   (a) R. Qiao, C. Yang and M. Gao, *J. Mater. Chem.*, 2009, **19**, 6274; (b) N. A. Frey, S. Peng, K. Cheng and S. Sun, *Chem. Soc. Rev.*, 2009, **38**, 2532; (c) D. Liu, W. Wu, X. Chen, S. Wen, X. Zhang, Q. Ding, G. Teng and N. Gu, *Nanoscale*, 2012, **4**, 2306.
6   (a) S. Sun and H. Zeng, J. Am. Chem. Soc., 2002, **124**, 8204; (b) T. Hyeon, *Chem. Commun.*, 2003, 927; (c) N. R. Jana, Y. Chen and X. Peng, *Chem. Mater.*, 2004, **16**, 3931.
7   (a) J. Xie, G. Liu, H. S. Eden, H. Ai and X. Chen, *Acc. Chem. Res.*, 2011, **44**, 883; (b) J. Gao, H. Gu and B. Xu, *Acc. Chem. Res.*, 2009, **42**, 1097; (c) Z. Zhou, C. Wu, H. Liu, X. Zhu, Z. Zhao, L. Wang, Y. Xu, H. Ai and J. Gao, *ACS Nano*, 2015, **9**, 3012.
8   (a) G. Palui, F. Aldeek, W. Wang and H. Mattoussi, *Chem. Soc. Rev.*, 2015, **44**, 193; (b) S. Jiang, K. Y. Win, S. Liu, C. P. Teng, Y. Zheng and M.-Y. Han, *Nanoscale*, 2013, **5**, 3127; (c) K. E. Sapsford, W. R. Algar, L. Berti, K. B. Gemmill, B. J. Casey, E. Oh, M. H. Stewart and I. L. Medintz, *Chem. Rev.*, 2013, **113**, 1904.
9   (a) M. H. Stewart, K. Susumu, B. C. Mei, I. L. Medintz, J. B. Delehanty, J. B. Blanco-Canosa, P. E. Dawson and H. Mattoussi, *J. Am. Chem. Soc.*, 2010, **132**, 9804; (b) A. M. Smith and S. Nie, *J. Am. Chem. Soc.*, 2008, **130**, 11278.
10 (a) C. Xu, K. Xu, H. Gu, R. Zheng, H. Liu, X. Zhang, Z. Guo and B. Xu, *J. Am. Chem. Soc.*, 2004, **126**, 9938; (b) K. Cheng, S. Peng, C. Xu and S. Sun, *J. Am. Chem. Soc.*, 2009, **131**, 10637; (c) D. Ling, W. Park, Y. I. Park, N. Lee, F. Li, C. Song, S.-G. Yang, S. H. Choi, K. Na and T. Hyeon, *Angew. Chem. Int. Ed.*, 2011, **50**, 11360; (d) H. B. Na, G. Palui, J. T. Rosenberg, X. Ji, S. C. Grant and H. Mattoussi, *ACS Nano*, 2012, **6**, 389; (e) H. Wei, N. Insin, J. Lee, H.-S. Han, J. M. Cordero, W. Liu and M. G. Bawendi, *Nano Letters*, 2012, **12**, 22. (f) Y. Liu, T. Chen, C. Wu, L. Qiu, R. Hu, J. Li, S. Cansiz, L. Zhang, C. Cui, G. Zhu, M. You, T. Zhang and W. Tan, *J. Am. Chem. Soc.*, 2014, **136**, 12552.
11 P. Zhang, S. Liu, D. Gao, D. Hu, P. Gong, Z. Sheng, J. Deng, Y. Ma and L. Cai, *J. Am. Chem. Soc.*, 2012, **134**, 8388.
12 S. K. Yen, D. Jańczewski, J. L. Lakshmi, S. B. Dolmanan, S. Tripathy, V. H. B. Ho, V. Vijayaragavan, A. Hariharan, P. Padmanabhan, K. K. Bhakoo, T. Sudhaharan, S. Ahmed, Y. Zhang and S. Tamil Selvan, *ACS Nano*, 2013, **7**, 6796.
13 L. Tang, T. M. Fan, L. B. Borst and J. Cheng, *ACS Nano*, 2012, **6**, 3954.
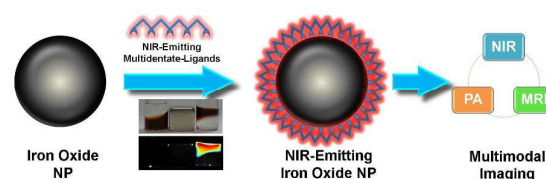14   Z. Xu, C. Shen, Y. Hou, H. Gao and S. Sun, *Chem. Mater.*, 2009, **21**, 1778.

Table of Contents：Compact NIR-active iron oxide nanoparticles protected by near-infrared catechol-multidentate polymers for NIRF/PA/MR trimodal imaging